Ultrafast study of carbonaceous hole transport materials for perovskite solar cell

A thesis submitted towards the partial fulfilment of BS-MS programme

(2015-2020)

By

Chandan Shekhar

20151151

Under the guidance of

Dr. Pankaj Mandal

Department of Chemistry

Indian Institute of Science Education and Research Pune

Pune, INDIA

Certificate

This is to certify that this dissertation entitled "**Ultrafast study of carbonaceous hole transport materials for perovskite solar cell**" towards the partial fulfilment of the BS-MS dual degree programme at the Indian Institute of Science Education and Research, Pune represents study/work carried out by **Chandan Shekhar** at Indian Institute of Science Education and Research under the supervision of **Dr. Pankaj Mandal**, Department of Chemistry, during the academic year 2019-2020.

.

Dr. Pankaj Mandal

Committee:

Supervisor - Dr. Pankaj Mandal

TAC - Dr. Angshuman Nag

This thesis is dedicated to everyone

Declaration

I hereby declare that the matter embodied in the report entitled "**Ultrafast study of carbonaceous hole transport materials for perovskite solar**" cell are the results of the work carried out by me at the Department of Chemistry, Indian Institute of Science Education and Research, Pune, under the supervision of Dr. Pankaj Mandal and the same has not been submitted elsewhere for any other degree

Chandan Shekhar

Date: 05.04.2020

Table of Contents

List of Tables

List of Abbreviations

GO	Graphene Oxide
rGO	Reduced Graphene Oxide
$CsPbBr_3$	Cesium lead bromide
$FAPbBr_3$	Formamidinium lead bromide
NC	Nano crystals
QD	Quantum Dots
XRD	X-Ray Diffraction
TEM	Transmission Electron Microscopy
PSC	Perovskite Solar cell
OA	Oleic acid
OLA	Oleylamine
ODE	Octadecene
PL	Photoluminescence
TRPL	Time-Resolved Photoluminescence
PSK	Perovskite
HEL	Hole Extraction Layer
HTM	Hole Transporting Material

List of Figures

Abstract

In the recent years, Perovskite solar cells (PSCs) have emerged as a better option to traditional solar cell technologies due to their thrilling optoelectronic properties. In a short time-span, recent advancements have led to increased power conversion efficiency from 3.9% to 23.8%. A typical perovskite solar cell structure involves an active perovskite absorber layer sandwiched between electron and hole transport layers (ETL and HTL) . These hole or charge-transporting layers help in efficient and irreversible separation of the electrons and holes photoexcited in the perovskite. Two different perovskites (organic ($FAPbBr_3$, formamidinium lead bromide) and inorganic ($CsPbBr_3$, cesium lead bromide) and hole-transporting materials (graphene oxide and reduced graphene oxide) were taken to measure and compare the Photoluminescence and transient Photoluminescence decays. Different samples of perovskites with hole-transporting materials of various concentrations were prepared. It was observed that rGO (reduced graphene oxide) came out to be a better hole transporting material than GO (graphene oxide). Because of GO (graphene oxide) getting reduced to rGO (reduced graphene oxide), reducing the oxygen containing groups which made slower hole injection from PSK (perovskite) to rGO (reduced graphene oxide) occurred in the global graphene structure, but delocalized holes in the benzene rings decreased the charge recombination to improve the efficiency of the rGO (reduced graphene oxide) based composites relative to the GO (graphene oxide) composites .

Acknowledgment

As I begin to write here, I realized that my stay at IISER Pune is going to end soon. This five years journey at IISER is going to be memorable because of several peoples. First of all, I would first like to express my sincere gratitude to my thesis supervisor Dr. Pankaj Mandal at IISER Pune. The door to his office was always open whenever I ran into a trouble spot or had a question about my research or writing . He consistently allowed this paper to be my own work, but steered me in the right direction whenever he thought I needed it.

I would also like to thank Dr. Angshuman Nag, Dr. Pramod Pillai, and Dr. Parth Hazra for letting me use their equipment. I owe my gratitude to all faculty members of the Physics and Chemistry Department at IISER Pune for the courses taught during my academic program, which also played a significant role for the completion of this thesis. I would also like to acknowledge my lab members especially Aman Chaturvedi and Avinash Warankar for their continuous efforts and help. I pass my sincere gratitude to my parents for their unconditional love, guidance, money and helping me to stand on my feet.

This journey would have been boring and lonesome without my friends who became my family in the due course. At last, I would like to thank myself for keeping the patience and not giving up.

Thank You!

Chandan Shekhar

20151151

Chapter 1 Introduction

Perovskite is a material with equivalent structure as CaTiO3. Pure perovskites have a general formula of AMX_3, where A and M are cations and X is an anion that binds to each cation [1]. In a typical structure, M is coordinated to six X anions, A is coordinated to twelve X anions.

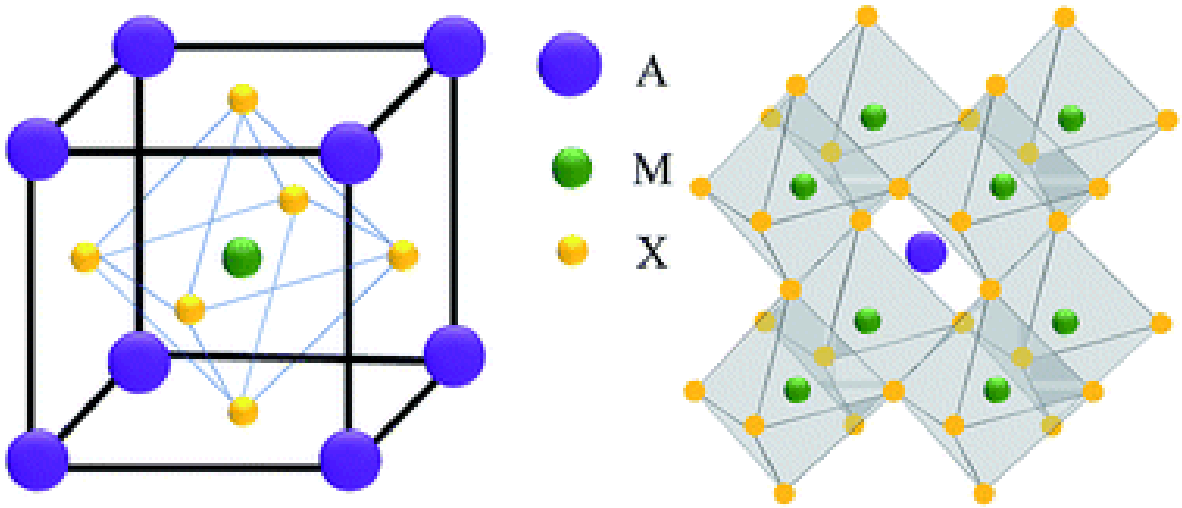

Figure 1: Source[2].Crystalline structure of inorganic–organic hybrid lead perovskite AMX_3

Perovskites comprise of anionic M-X semi-conductive frameworks and charge-compensating cations. Complex structures supported by a Nano-scale composite of inorganic and organic parts, offer an interesting possibility of crafting different useful materials for further research and applications. Inorganic materials, generally characterized with ionic and covalent interactions, offer a potential for high electrical mobility, with a wide range of band gaps (enabling the structure of insulators, semiconductors, metals, and superconductors), attention-grabbing magnetic interactions, a wide range of non-conductor properties, substantial mechanical hardness, and thermal stability. On the other hand, Organic molecules that usually interact through weaker interactions like hydrogen bonding and van der Waals interactions, offer a chance of structural diversity, extremely efficient luminescence, a large degree of polarizability, plastic mechanical properties, and in some cases it is conducting or superconducting[3]. Usually, organic-inorganic hybrid analysis focuses on using the vary of interactions found among organic and inorganic chemistry to make a composite with some unique properties not accomplishable with organic or inorganic materials alone, or to mix

helpful properties of the 2 parts in one single material. Recent advances in organometallic halide perovskites, have attracted greater interest attributable to their spectacular photovoltaic phenomenon and straightforward device producing processes that have a huge potential for commercial applications [4]. Over the past six years, PSCs have experienced unprecedented development in power conversion efficiency (PCE) with performance soaring to over 22%[5] . Moreover in the past few years, continuous efforts have been dedicated to realizing PSCs with even higher performance. As the heart of PSCs, hybrid ABX3 organic–inorganic halide perovskites possess ideal photovoltaic properties such as optimal band gaps (~1.5eV), high absorption coefficients, long carrier diffusion lengths[6] . In addition to solar cells, organometallic perovskites have also been incorporated into many optoelectronic instruments such as light-emitting diodes, lasers, and photo-diodes[7] .

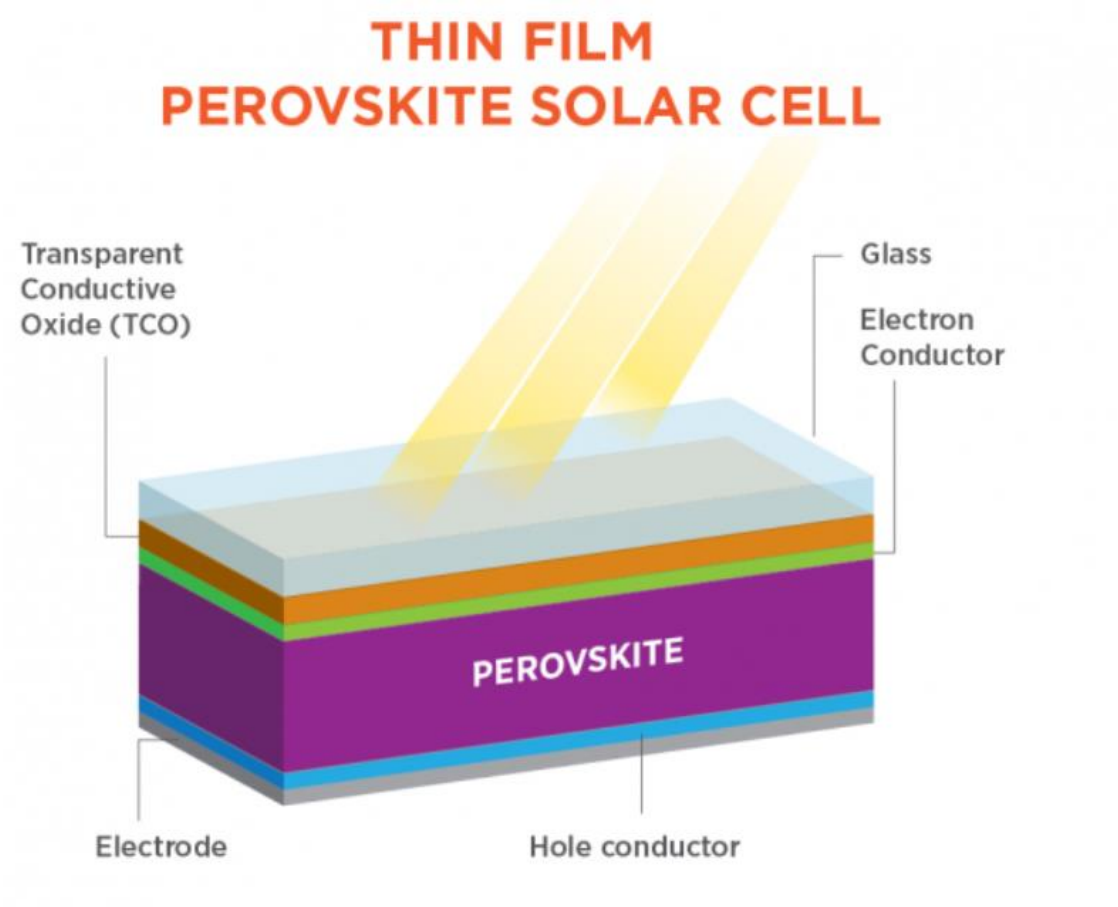

Figure [2]: Source[8], Represents the structure of thin film perovskite solar cell

The charge carriers are created in the perovskite layer after the incident photons are absorbed under illumination. The charging carriers are then immediately moved through the transport channels including the ETM / HTM layers, passing each interface between them, and finally extracted from the PSC anode and cathode [9, 10]. The distinctly tortuous

path of electrons and holes requires a well-constructed layered structure to prevent quenching or recombination of the carriers during their movement. During the transport process, traps and defects in perovskite films and ETM / HTM layers can catch or recombine the free carriers due to their internal imperfections. PSCs poor long-term stability is primarily due to perovskite's existing susceptibility to moisture, light, and heat. The proper design of interfacial layers in PSCs can isolate perovskite films effectively from exposure to these unwanted environments affects device stability[11].

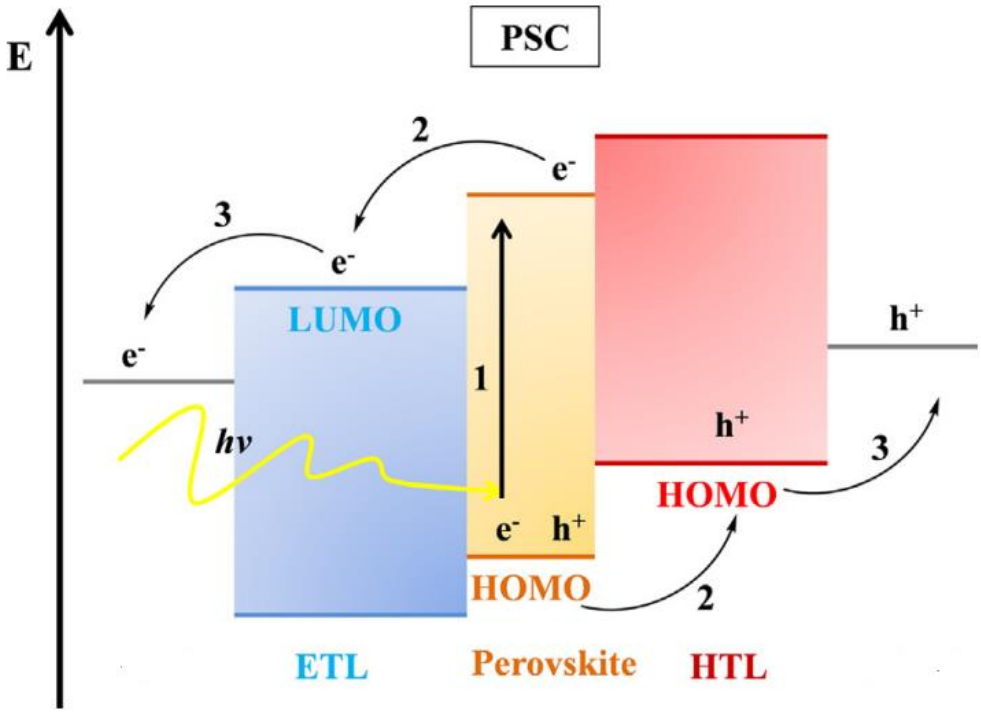

Figure [3]: Source [12], Band levels of basic structure of working PSC

Above Figure represents the band diagram of a complete structure of working perovskite solar cell (from 1. Generation of free charges due to absorption of photon, 2. Charge or hole transportation to HOMO or LUMO, 3. Charge extraction from HOMO or LUMO to further substrate generating potential difference).

For many reasons, dealing with electron capture and transport is a bigger problem in photovoltaic devices . In PSCs, the duration of the electron diffusion is relatively shorter than that of the holes which leads to a greater chance of quenching [15]. While perovskite can act as both an effective light harvester and a hole transporter in HTM- PSCs, the presence of an HTM will further facilitate the transport of hole from perovskites to anodes for better performance for devices [16]. In order to ensure long-term stability of high-performance PSCs, it is imperative to create new HTMs with decent hydrophobicity, compact

morphology, suitable energy level compatibility with perovskites, fast hole transport rate, good optical clarity and low cost.

To improve the photovoltaic parameters and thereby to improve the performance of the system. Hole Transport Materials (HTMs) can be classified into different types: organic, inorganic and carbonaceous HTMs (based on how they interact with each other). To understand the role of HTM in detail, it can be further divided into different subgroups.

Stability and performance depend on the transport layers used in the system architecture, as it serves the different facts of PSCs such as; (i) functions as a physical / energy barrier between ETL and perovskite layer by preventing the flow of electrons; (ii) improving the efficiency of the hole transport due to its high hole mobility and matching energy levels with those of ETMs / HTMs and electrode; (iii) Evitates the deterioration and corrosion that can occur where there is no HTM at the metal-perovskite interface (iv) suppresses recombination of charges by removing the top surface entirely from the bottom transport or surface layer resulting in better performance [13].

This will have a sufficient level of energy, supplying the driving force for the transfer of charge (i.e. the maximum occupied molecular orbital, HOMO, energy levels of the chosen HTMs must be marginally higher than those of the perovskite material). This serves as a shield to block electrons between anode and perovskite substrate without reaching the anode. But the instability-related issues with using HTMs based on these organic long chain polymers remain a concern. This spiro-OMeTAD as HTM often includes costly additives (4-tert-butylpyridine) and dopants (typically hygroscopic li-salts), as it suffers from low spiro-structure instability. To address these drawbacks the spiroskeleton should be replaced with other ensemble to increase the reliability of the perovskite / HTL interface. Because performance and stability in photovoltaics are both important, the inorganic HTMs provide inexpensive stability but remain unsatisfied in terms of efficiency. Whereas maintaining both performance and reliability using one HTM is an important feature. Thus, in terms of performance and long-term stability, carbon has been described as a possible HTM.

Carbonaceous materials are successful HTMs because of their low-cost, good connectivity and the unusual property of showing good mechanical strength and adhesion to the film minimizing the resistance of the interface in solar cells. Their work-function value (approximate 5.0 eV) also makes them an ideal material for replacing the role of HTMs in PSCs [14].

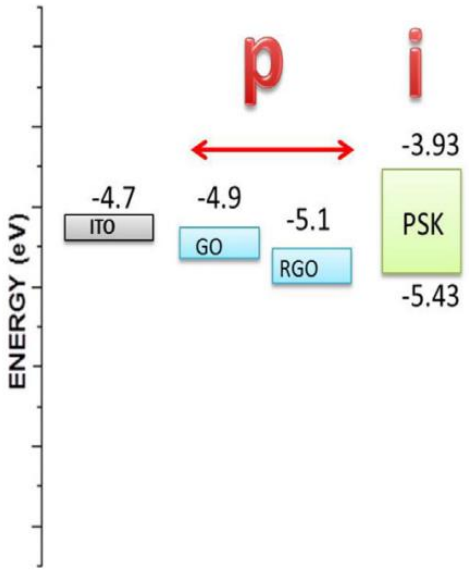

Figure [4] Source [12]:, Represents the band alignment of perovskite (PSK) with GO and rGO

Also, a systematic analysis of the mechanisms is responsible for improving the performance of r-GO devices. It has been showed that facilitated charging with delayed recombination, high r-GO conductivity, better balanced energy rates and better growth of perovskites on r-GO HTMs are responsible for high efficiency [17]. The increase in PCE in r-GO based PSCs can be attributed to the reduction of the number of charged bulk defects within the perovskite layer due to the light illumination during measurements

Chapter 2 Materials and Methods

Chemicals:

Cesium carbonate (Aldrich, 99.9%), lead (II) bromide (99.999%, Aldrich), PbBr2, Oleylamine (OAm, technical grade 70%, Aldrich), 1-Octadecene (ODE, technical grade 90%,Aldrich), toluene (99.5%, Rankem), Formamide (FA, spectroscopy grade, Aldrich), Graphite flakes, Potassium permanganate (KMnO4), Hydrochloric acid (99.999%, Aldrich), Sulfuric acid (99.999%, Rankem), Iron(II) chloride ($FeCl_2$) were used. All the chemicals were used without any further purification.

Synthesis of Graphene Oxide:

Graphene oxide, which is used as charge trapping layer in a perovskite solar cell, was synthesised using modified Hummer's method. 1g of powdered graphite flakes was stirred with 20mL of conc. H_2SO_4 for 1hr at (<5 °C) ice bath. Then 3g of $KMnO_4$ was added slowly (in 30 min) and continuously stirred for 24hr at room temperature. Following, 40ml of MQ water was slowly added with continuous stirring. It was stirred again at 80°C for 3hr and then left for getting it back to RT (room temperature). Finally a water-hydrogen-peroxide solution (120mL of H_2O +10ml of H_2O_2) was added and left for few hours. The final solution was washed with H_2O, 5% HCl solution and finally with acetone. The resulting chocolate brown coloured material which was Graphene Oxide was extracted and dried under vacuum for 24 hr at 70°C.

Synthesis of reduced Graphene oxide:

Graphene oxide, prepared from the above mentioned process, was further exfoliated in MQ water to make 1mg/ml solution (1.5g of GO taken). After that, 1.8g of $FeCl_2$ was added into 180mL of aqueous HCl solution (150mL of H_2O + 30mL of HCl) and further mixed with 150mL of GO solution (of 1mg/mL solution). Then it was stirred for 24hr at 94 °C. The final black coloured precipitate was filtered and washed with H_2O and small amount of methanol, and finally dried under hot oven.

Synthesis of Cs-oleate as a cesium precursor:

0.407 g (1.25 mmol) Cs_2CO_3, 1.25 mL OA and 20 mL ODE were taken in 50 mL 3-necked round bottom flask and the mixture was kept under vacuum for 30 min at 120 ^{o} C followed by purging with N2 for 10 min along with mild magnetic stirring. This process of alternate application of vacuum and N2 was repeated for 3 times to achieve the removal of moisture and O2 from the reaction mixture. The temperature was increased to 150 ^{o} C and the reaction was continued until the Cs_2CO_3 got dissolved to give a clear solution after reacting with OA. The as-synthesized Cs-oleate solution in ODE was kept as cesium precursor for synthesis of $CsPbBr_3$ nanocrystals (NCs).

Synthesis of colloidal $CsPbBr_3$ NCs:

Colloidal NCs of $CsPbBr_3$ of two different sizes were synthesized following a recent report. 5ml of ODE which was dried under vaccum and 0.069 g (0.188 mmol) of $PbBr_2$ were taken into 50 mL 2-necked round bottom flask. The mixture was degassed (under alternate vacuum and nitrogen) at 120 ºC for 60 minutes along with magnetic stirring. Dried OA and OAm, each 0.5 mL, was added to the mixture at 120ºC. After 30 min, $PbBr_2$ get dissolved in ODE and then the temperature was increased to 190 º C. As synthesized Cesium-oleate (0.1M, 0.4 mL) solution in ODE, pre-heated at 100º C, was slowly injected to the reaction mixture . The reaction mixture became greenish and the reaction was stopped by dipping the reaction flask into an ice bath . The synthesized cesium lead bromide NCs were collected by adding 5 ml tert-butanol at room temperature and then centrifuged at 9000 rpm .Finally, the NCs obtained were redispersed in 5 ml toluene for characterization.

Synthesis of $FAPbBr_3$ (Formamidinium Lead Bromide) nanocrystals:

Nanocrystals (NCs) were synthesised using following method:

Preparation of FA-oleate as FA precursor:

Formamidinium acetate (5 mmol, 0.521 g), was loaded into a 100 mL 3-neck flask along with dried oleic acid (20 mL, OA,). Then reaction was mixed under vacuum and dried at 120 ºC. And then again it was heated under N_2 at 130 ºC until the reaction completed, and then again dried for 30 min at 50 ºC under vacuum.

Synthesis of $FAPbBr_3$ NCs:

This synthesis method was an adaptation of earlier mentioned synthesis of $CsPbBr_3$ NCs. So, again 5mL dried ODE and 0.069 $PbBr_2$ (lead bromide) were taken in a 50 mL 3-necked round bottom flask, and degassed at 120°C for 60 min under alternate vacuum and nitrogen. Dried OLA (0.5 mL) and dried OA (1 mL) were injected at 120 ºC under N_2 environment. When the solution became clear, after the complete solubilization of $PbBr_2$ salt the temperature was raised to 110 ºC. Then the earlier prepared FA-oleate solution (2.5mL, .25M) was injected and just after 5sec, reaction mixture was cooled by ice bath. The extracted solution, 10 mL of toluene and 5 mL of acetonitrile were added and the mixture was centrifuged for 2:30 min at 9000 rpm. The supernatant was discarded and the precipitate was re-dispersed in 5 mL toluene.

Chapter 3 Experimental Design

Two different types of perovskite were taken, (i) Cesium Lead Bromide ($CsPbBr_3$), (ii) Formamidinium Lead Bromide ($FAPbBr_3$). Carbonaceous materials used as hole transporting material (HTM)/ hole transporting layer (HTL) were, Graphene Oxide (GO) and Reduced Graphene Oxide (rGO)

Ten different thin films/ composites were prepared with perovskites and HTMs and characterization were done:

(i) $CsPbBr_3$
(ii) $CsPbBr_3$/GO (2mg/ml)
(iii) $CsPbBr_3$/GO (1mg/ml)
(iv) $CsPbBr_3$/rGO (2mg/ml)
(v) $CsPbBr_3$/rGO (1mg/ml)
(vi) $FAPbBr_3$
(vii) $FAPbBr_3$/GO (2mg/ml)
(viii) $FAPbBr_3$/GO (1mg/ml)
(ix) $FAPbBr_3$/rGO (2mg/ml)
(x) $FAPbBr_3$/rGO (1mg/ml)

Film deposition of graphene oxide and reduced graphene oxide was done by Doctor's blading method, and deposition of perovskite was performed by spin coating at 5000rpm.

Chapter 4 **Results and Discussion**

Graphene oxide (GO) and reduced graphene oxide (rGO) were synthesized with the modified Hummer's method. The product obtained was were examined and confirmed using pXRD technique and Raman spectra.

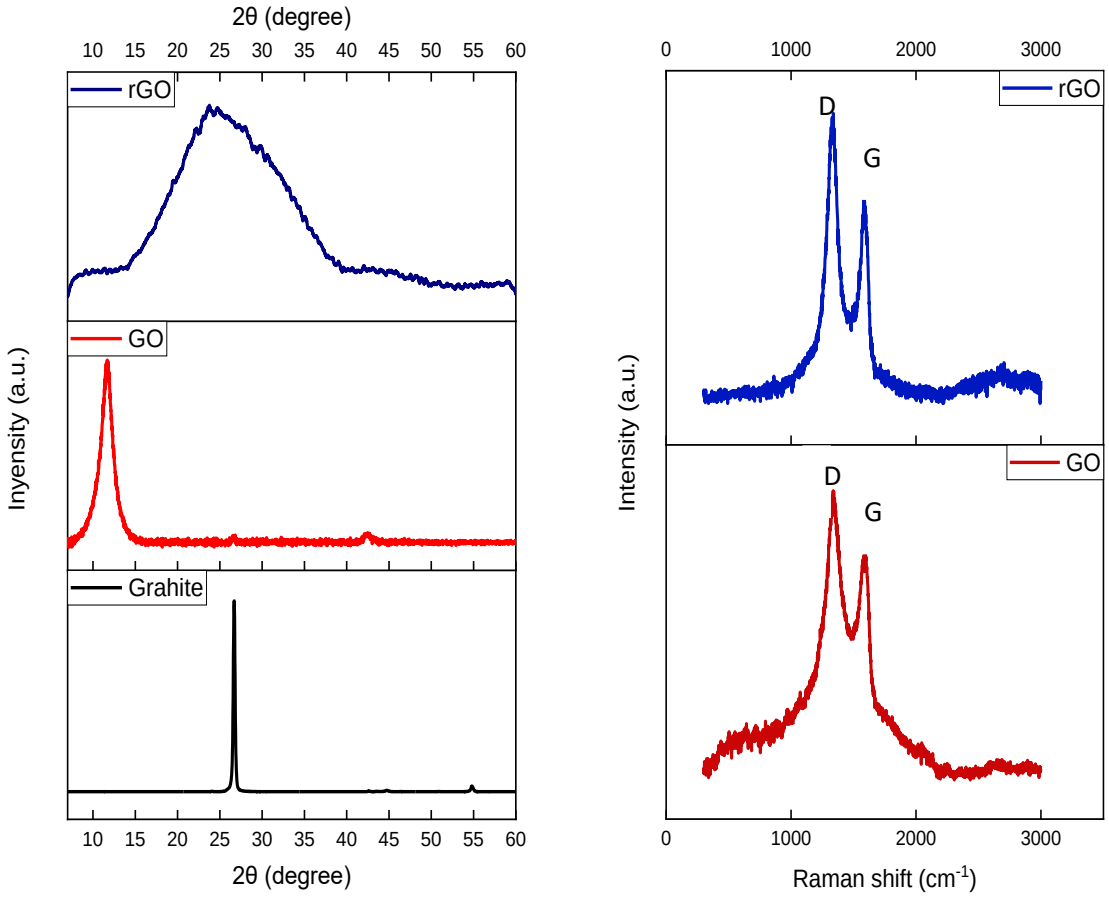

(a) **(b)**

Figure [5]: (a) pXRD pattern for Graphite, Graphene Oxide and reduced Graphene Oxide (b) Raman spectra for Graphene Oxide and reduced Graphene Oxide

A clear X-ray diffraction powder (PXRD) peak graphite point (002) emerged at 2θ = 26.4° (d equivalent to ~0.339 nm). After oxidation of graphite flakes, the oxide groups (-C=O/-C-O, -OH,-COOH) fully covered the graphite sheets and strongly repelled each other apart, and accordingly the (002) peak appeared at 2θ = 10.7° with greater interlayer distance of equivalent to ~0.825 nm. But after reduction it made graphene sheets less oxygenated, but many defects may have been produced in the process of reduction since few of the carbon atoms are still sp3 hybridised. A wide peak occurred in rGO's pXRD pattern with maximum peaks around 2θ = 22.5° and interlayer spacing about 0.391 nm.

Two significant large bands appeared in Raman's spectra of both GO and rGO materials: a D band (defect peak due to interval scattering) at 1,330 cm^{-1} and a G band (graphene G peak) appeared at 1,590 cm^{-1}. The peak intensity ratios (I_D / I_G) were found to be about 2.65 and 2.42 for GO and rGO, respectively, and the decline in the strength ratio (I_D / I_G) indicates a recovery of the sp^2.

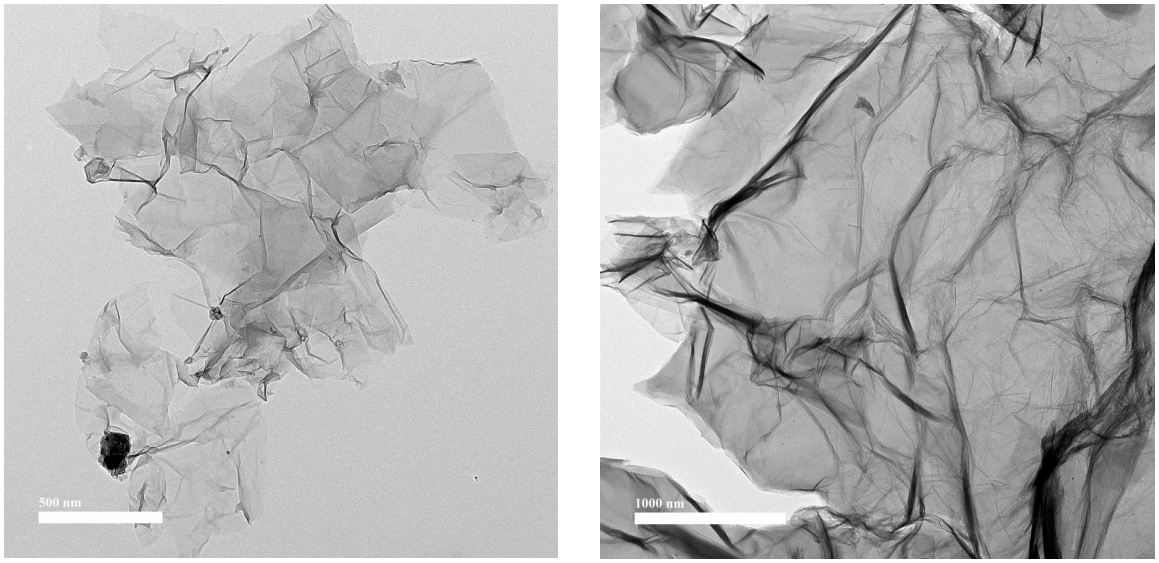

(a)

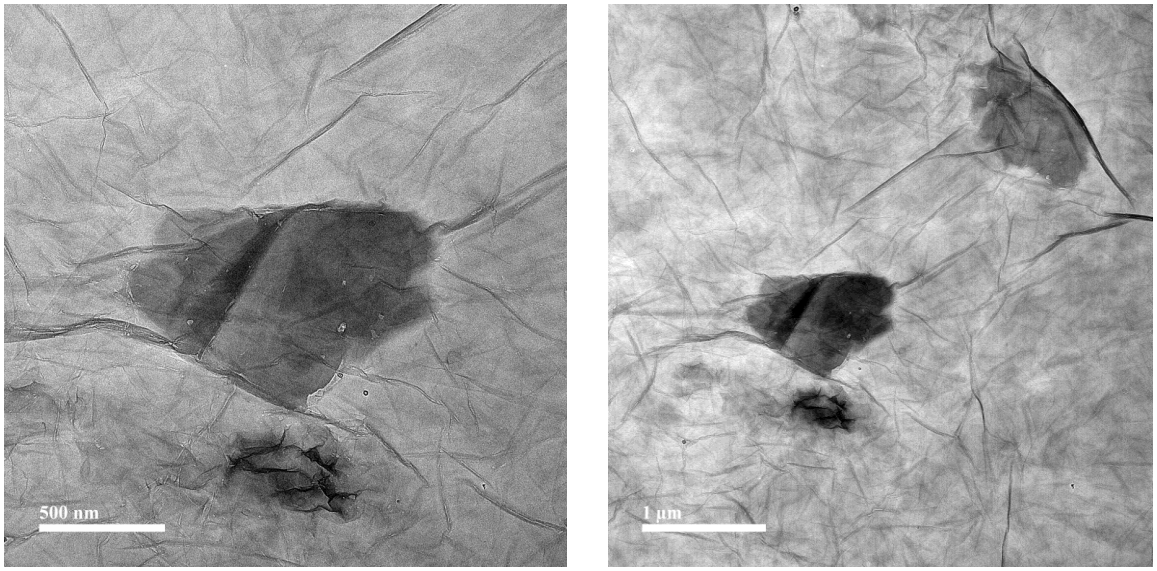

(b)

Figure [6]: TEM images of thins films of (a) GO (500nm), (b) GO (1000nm), (c) rGO (500nm) and (d) rGO (1000nm).

The reaction procedure that used to produce a few layers of GO and rGO as evident from the, and transmission electron microscopy (TEM) images[15].

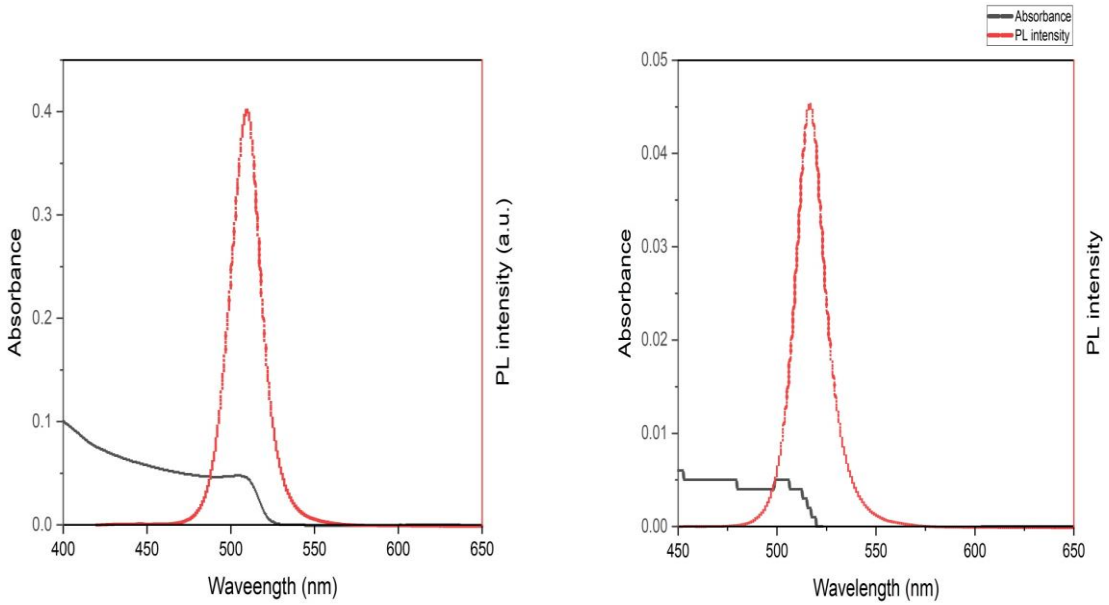

(a) $CsPbBr_3$ **(b)** $FAPbBr_3$

Figure [7]: Photoluminescence (PL) spectra and absorbance spectra for (a) $CsPbBr_3$ (b) $FAPbBr_3$ QDs

The pixelated plot of perovskites for absorbance spectra represents the concentration used was too less. For $CsPbBr_3$ PL spectra peak was observed at 524nm, similarly for $FAPbBr_3$ peak was at 543nm.

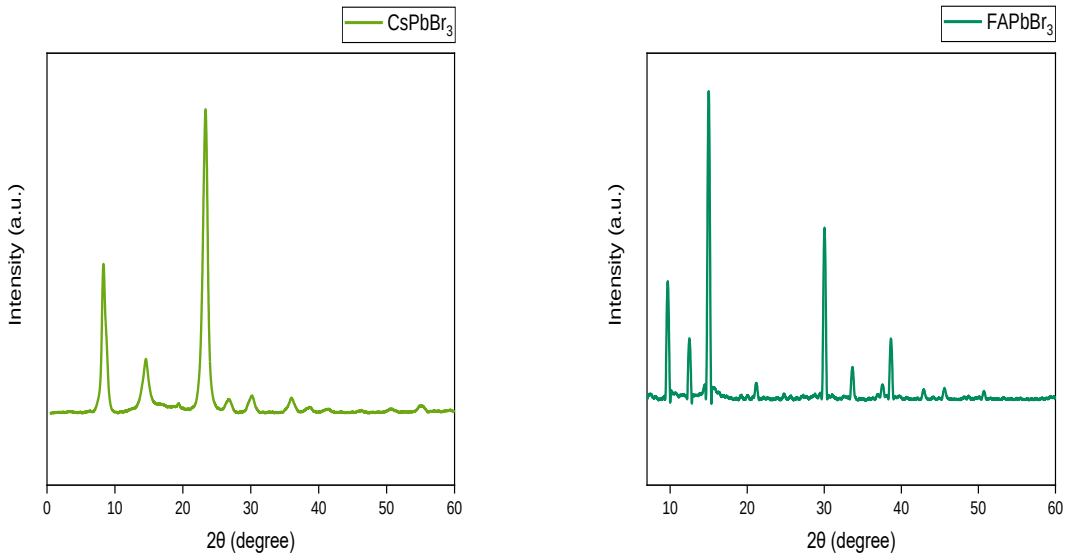

(a) **(b)**

Figure [8]: pXRD pattern for (a) $CsPbBr_3$ and (b) $FAPbBr_3$

The crystallinity for the quantum dots prepared were confirmed from reported result [25, 26].

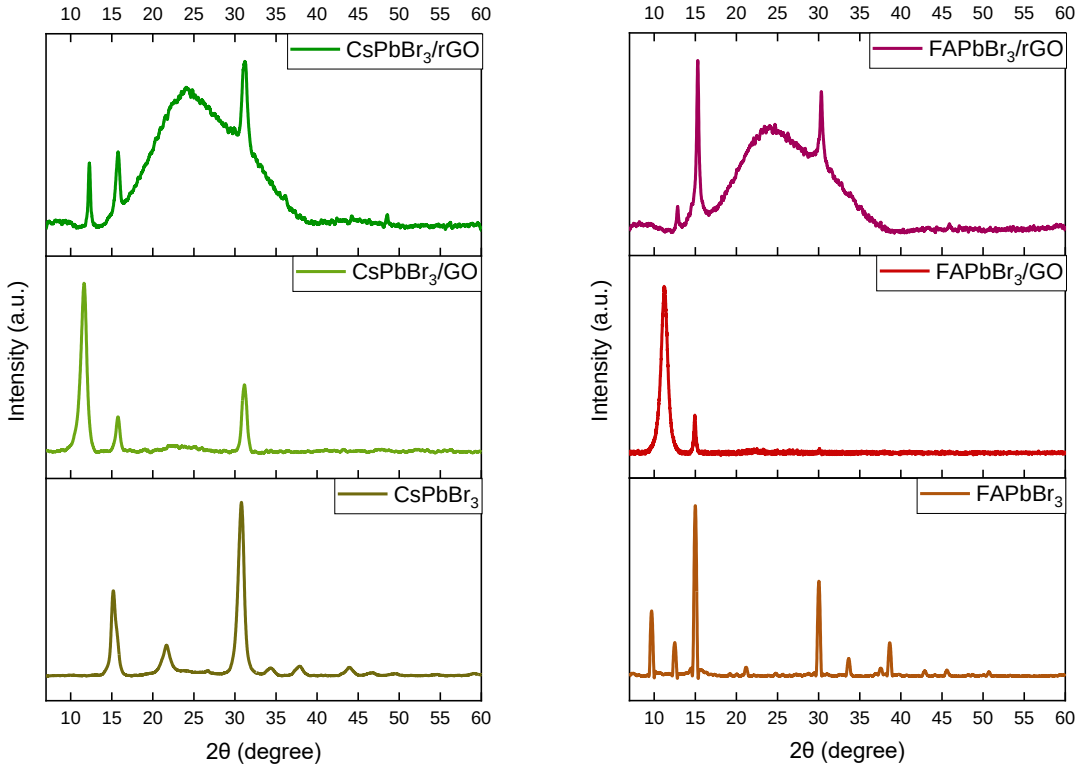

(a) **(b)**

Figure [9]: pXRD pattern for (a) $CsPbBr_3$ composite with GO and rGO (b) $FAPbBr_3$ composite with GO and rGO.

pXRD patterns confirmed that all the composites prepared were properly deposited with quantum dots ($CsPbBr_3$ and $FAPbBr_3$) and hole transporting materials (graphene oxide and reduced graphene oxide) .

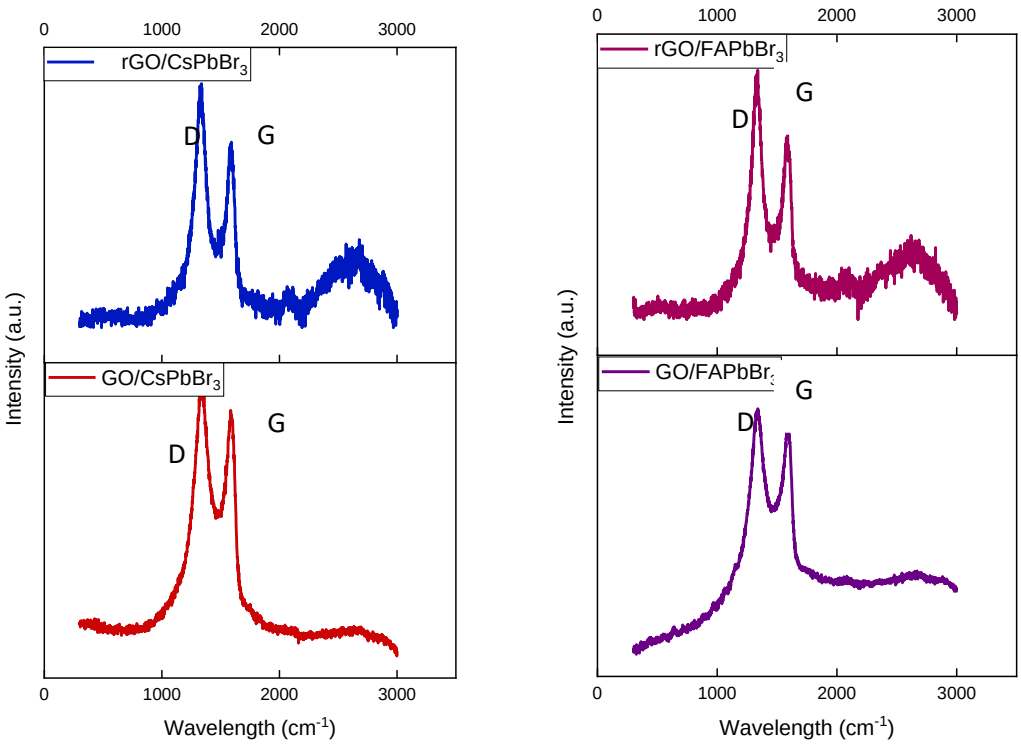

(a) **(b)**

Figure [10]: Raman Spectra for (a) composite of $CsPbBr_3$ with GO and rGO (b) composite of $FAPbBr_3$

Above Raman Spectra of samples also confirms that composites with graphene oxide and reduced graphene oxide.

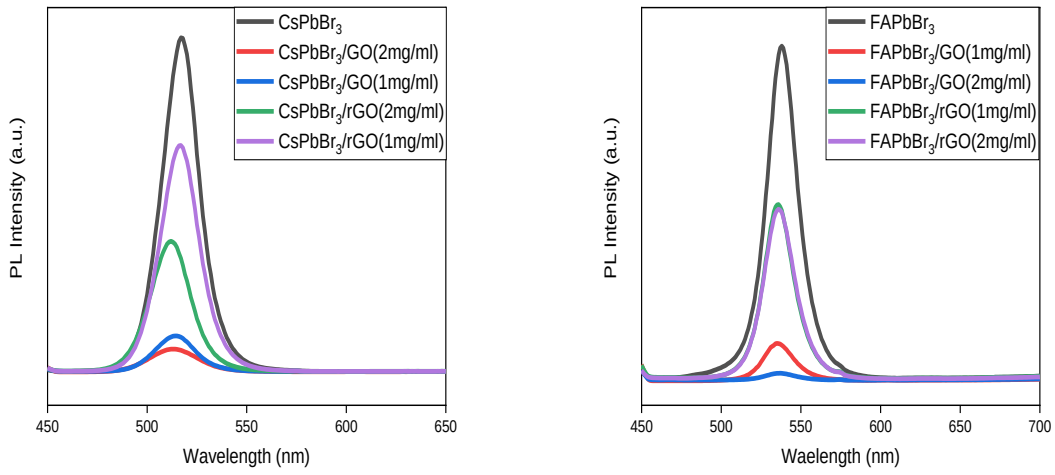

(a) **(b)**

Figure [11]: Photoluminescence (PL) spectra for composites of (a) $CsPbBr_3$ and (b) $FAPbBr_3$ with different concentrations of GO (2mg/ml and 1mg/ml) and rGO (2mg/ml and 1mg/ml), PSK(perovskite)

Relative to the perovskite samples, a strong quenching of PL intensities can be observed in Figure [11] and for the bilayer samples with the perovskite layer in either GO or rGO, used as hole transporting layers HEL. However, as seen in Figure [11], the effect of PL quenching is more pronounced for GO than for other rGO layers; the PL intensities indicate an order : ITO / $CsPbBr_3$> ITO/rGO(1mg/ml)/ $CsPbBr_3$> ITO / rGO(2mg/ml)/ $CsPbBr_3$> ITO/GO(1mg/ml)/ $CsPbBr_3$> ITO/GO(2mg/ml) . This finding shows that rGO has a better hole-extraction feature than other GO layer to efficiently quench the PL intensity. The PL intensities are known to be indirect indicators for the lifetime of the excitons released in these samples, but direct evidence emerged from measurements of these sample PL decay kinetics.

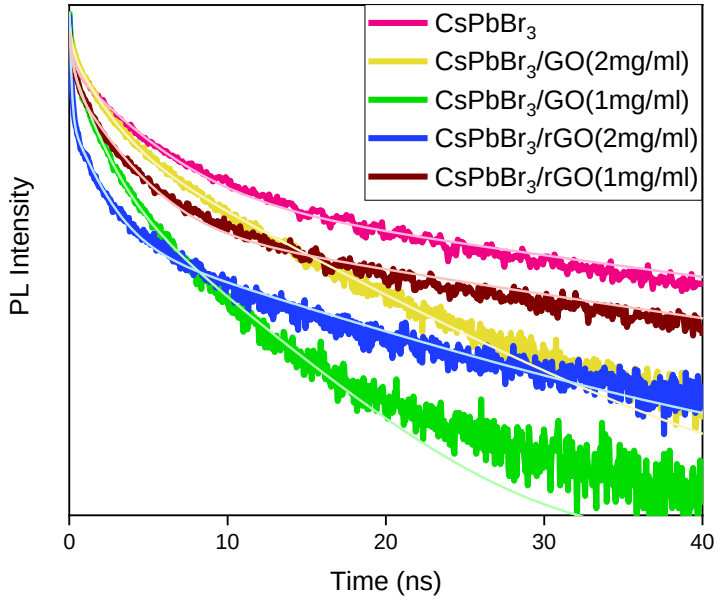

Figure [12]: Transient PL decay profiles of $CsPbBr_3$ on glass substrate on varied concentration with GO and rGO as indicated

Sample	**A_1**	**τ_1/ns**	**A_2**	**τ_2/ns**	**A_3**	**τ_3/ns**	**τ_{PL}/ns**	**τ_h/ns**
$CsPbBr_3$	0.28363	0.2397	0.34584	3.69989	0.08077	31.80855	5.51466	-
$CsPbBr_3$/GO(2mg/ml)	0.27264	0.1709	0.36552	1.81061	0.18296	8.76481	2.81568	6.812546
$CsPbBr_3$/GO(1mg/ml)	0.43962	0.10587	0.36423	1.3622	0.11123	5.56387	1.26936	5.562804
$CsPbBr_3$/rGO(2mg/ml)	0.66635	0.10241	0.16912	1.5575	0.04433	13.95476	1.08008	7.045253
$CsPbBr_3$/rGO(1mg/ml)	0.30291	2.56906	0.32423	0.26057	0.05361	27.42883	3.427305	9.025473

Table [1]: Time coefficients and relative amplitudes of corresponding perovskite films, perovskite films with composite obtained from fitting PL transients for perovskite $CsPbBr_3$

The normalized transient PL decay intensity of the respective samples are seen in Figure, indicating the pattern of decay the same as the pattern of PL decay. All TRPL (time-resolved Photoluminescence) decay were fitted with Exponential decay function 2 in OriginLab, the respective lifetimes and relative amplitudes are summarized in the given table below. It can be said that the first decay component is due to the non-radiative relaxation of the surface state in the grain boundaries of the perovskite and the second and third decay component is due to the radiative recombination or non-radiative relaxation in the bulk .

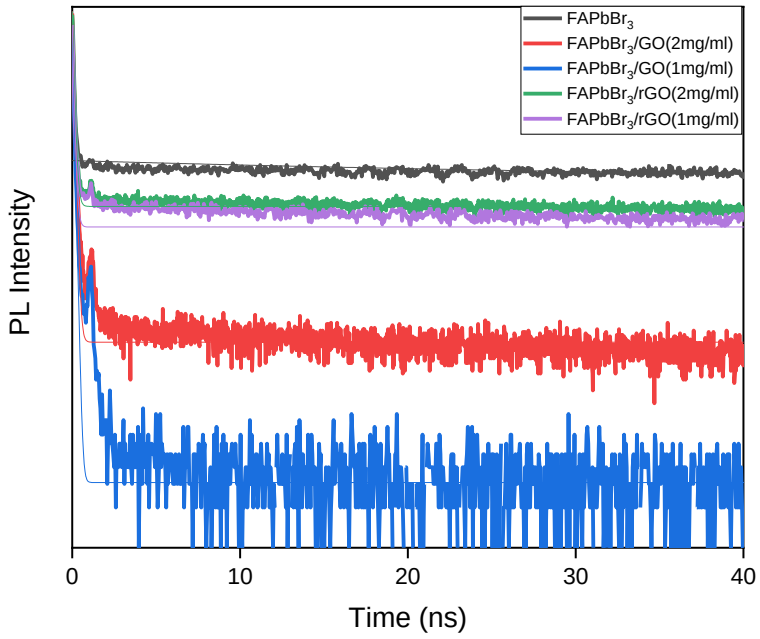

Figure [13]: Transient PL decay profiles of $FAPbBr_3$ on glass substrate on varied concentration with GO and rGO as indicated

Sample	**A_1**	**τ_1/ns**	**τ_{PL}/ns**	**τ_h/ns**
$FAPbBr_3$	0.02466	38.0528	38.0528	-
$FAPbBr_3$/GO(2mg/ml)	1.01716	0.091	0.091	0.091218
$FAPbBr_3$/GO(1mg/ml)	0.72678	0.08156	0.08156	0.081735
$FAPbBr_3$/rGO(2mg/ml)	0.98171	0.09766	0.09766	0.097911
$FAPbBr_3$/rGO(1mg/ml)	0.77871	0.09007	0.09007	0.090284

Table [2]: Time coefficients and relative amplitudes of corresponding perovskite films, perovskite films with composite obtained from fitting PL transients for perovskite $FAPbBr_3$

From the PL spectra it was confirmed that the concentration used wasn't enough to study the proper time-resolved decay of $FAPbBr_3$ and its composites. But still it can be observed that rGO came out to be an efficient hole extracting material than the GO.

The average PL lifetimes calculated with equation, $\tau_{PL} = \frac{\sum A_i \tau_i}{\sum A_i}$, here τ_i are time coefficients and are the corresponding amplitudes of each component.

The interfacial hole-extraction time (τh) at the interface between PSK and HEL can be predicted using the following equation, $\frac{1}{\tau_h} = \frac{1}{\tau_{PSK/HEL}} - \frac{1}{\tau_{PSK}}$, in which τ_{PSK} and τ_{PSK}/HEL are the PL lifetimes for perovskite only and those with perovskite deposited on varied hole transporting layer films, respectively.

Chapter 5 Discussion

It can be concluded from the transient photoluminescence decay plot that the first decay component is because of the non-radiative relaxation of the surface state in the grain boundaries of the perovskite and the second and third decay component to the radiative recombination or nonradiative relaxation in the bulk for the $CsPbBr_3$. However proper conclusion cannot be drawn for the $FAPbBr_3$ as the concentration used wasn't enough for the proper composite made. Decay coefficients decreased in a sufficient amount when the perovskite layer was in contact with the hole transporting layer of graphene oxide, reduced graphene oxide because of efficient hole transfer from perovskite to hole transporting layer . The consequent change of average photoluminescence lifetimes (τPL) of the composites shows the order of: ITO / PSK > ITO/rGO(1mg/ml)/ PSK > ITO / rGO(2mg/ml)/ PSK > ITO / GO (1mg/ml)/ PSK > ITO / GO(2mg/ml). Assuming that all PL quenches are due to the effect of hole extraction, evaluated hole extraction times (τ_h) shows the ability of hole extraction, indicating that GO is a more effective hole transporting layer as compared to all reduced graphene oxide. It can be assumed that hole extraction occurs quickly in graphene oxide due to the oxygen-containing functional groups which contribute to the electronic density to the hole of the excited perovskite so that the hole in PSK (perovskite) is extracted into the HEL more faster than hole extraction directly from the benzene rings on the surface of GO . If such oxygen groups are reduced, the hole extraction from perovskite to the hole transporting layer would be slowed. Although it can be said that the oxygen-containing functional groups on graphene oxide surface act as the hole-extraction sites (so that graphene oxide quenches the PL intensity efficiently). These oxygen-containing groups bonded to the tetrahedrally coordinated carbon atoms not only extract holes from the perovskite efficiently but also generate these holes localized on the oxygen atoms. By comparison, where certain oxygen containing groups were decreased in reduced graphene oxide, slower hole injection from perovskite to reduced graphene oxide could occur in the whole graphene structure, but delocalized holes in the benzene rings would delay charge recombination . However, further study can be done by applying ultrafast terahertz time domain spectroscopy and transient absorption techniques to understand carrier dynamics for hole injection. These ultrafast hole injection dynamics can provide comprehensive information about thetransfer mechanism, efficiency and time scales of hole transport across the Perovskite/HTL interface.

References

[1] Gonzalez-Carrero, Soranyel, et al. "Organic-Inorganic and All-Inorganic Lead Halide Nanoparticles [Invited]." *Optics Express*, vol. 24, no. 2, 2015, doi:10.1364/oe.24.00a285.

[2] Li, D., Liao, P., Shai, X., Huang, W., Liu, S., Li, H., … Wang, M. (2016). Recent progress on stability issues of organic–inorganic hybrid lead perovskite-based solar cells. *RSC Advances*, *6*(92), 89356–89366. doi: 10.1039/c6ra19801e

[3] Mitzi, D. B. (2007). Synthesis, Structure, and Properties of Organic-Inorganic Perovskites and Related Materials. *Progress in Inorganic Chemistry*, 1–121. doi: 10.1002/9780470166499.ch1

[4] Ye, M., He, C., Iocozzia, J., Liu, X., Cui, X., Meng, X., … Lin, Z. (2017). Recent advances in interfacial engineering of perovskite solar cells. *Journal of Physics D: Applied Physics*, *50*(37), 373002. doi: 10.1088/1361-6463/aa7cb0

[5] NREL 2016 Best research-cell efficiencies www.nrel.gov/ ncpv/images/efficiency_chart.jpg

[6] Dong Q, Fang Y, Shao Y, Mulligan P, Qiu J, Cao L and Huang J 2015 Science 347 967–70

[7] Masthead: (Adv. Mater. 27/2015). (2015). *Advanced Materials*, *27*(27). doi: 10.1002/adma.201570181

[8] https://www.energy.gov/eere/solar/perovskite-solar-cells

[9] Luo S D W A 2015 J. Mater. Chem. A 3 8992–9010

[10] Shi S, Li Y, Li X and Wang H 2015 Mater. Horiz. 2 378–405

[11] Meidan Ye et al 2017 J. Phys. D: Appl. Phys. 50 373002

[12] Marinova, Nevena, et al. "Organic and Perovskite Solar Cells: Working Principles, Materials and Interfaces." *Journal of Colloid and Interface Science*, vol. 488, 2017, pp. 373–389

[13] Marinova, N., Valero, S., & Delgado, J. L. (2017). Organic and perovskite solar cells: Working principles, materials and interfaces. *Journal of Colloid and Interface Science*, *488*, 373–389. doi: 10.1016/j.jcis.2016.11.021.

[14] Pitchaiya, S., Natarajan, M., Santhanam, A., Asokan, V., Yuvapragasam, A., Ramakrishnan, V. M., … Velauthapillai, D. (2020). A review on the classification of organic/inorganic/carbonaceous hole

transporting materials for perovskite solar cell application. *Arabian Journal of Chemistry*, *13*(1), 2526–2557. doi: 10.1016/j.arabjc.2018.06.006

[15] Xing G, Mathews N, Sun S, Lim S S, Lam Y M, Graetzel M, Mhaisalkar S and Sum T C 2013 Science 342 344–7

[16] Heo J H et al 2013 Nat. Photon. 7 487–92

[17] Yeo, J.-S., Kang, R., Lee, S., Jeon, Y.-J., Myoung, N., Lee, C.-L., … Na, S.-I. (2015). Highly efficient and stable planar perovskite solar cells with reduced graphene oxide nanosheets as electrode interlayer. *Nano Energy*, *12*, 96–104. doi: 10.1016/j.nanoen.2014.12.022

[18] Jha, P. K., Singh, S. K., Kumar, V., Rana, S., Kurungot, S., & Ballav, N. (2017). High-Level Supercapacitive Performance of Chemically Reduced Graphene Oxide. *Chem*, *3*(5), 846–860. doi: 10.1016/j.chempr.2017.08.011.